Detailed analysis of Triple-Axis Cross Pivot Elastic Pair

Design Assignment-1

ME254-2025

R.Vishwanath
25094

Contents

1 Objective

To perform kinetostatic analysis of triple-axis cross pivot elastic pair (TaCP) and obtain the following parameters:

- Intended-axis stiffness/compliance
- Full stiffness matrix (linearized at zero load)
- Range of rotation
- Axis-drift
- Extent of linearity

2 Geometry of triple-axis cross pivot

A schematic of the triple-axis cross-pivot with and without curved elements is shown in fig. 1. In general, the leaf-like segments undergo flexural deformation to allow torsional rotation of the elastic pair. The curved elements are incorporated in the design of high-accuracy cross-axis pivots as they can reduce axis drift and are more compliant in compassion to TaCP with straight elements [2].
The geometry described in Serafino et al. [2] is shown in fig. 2a, and the geometry model of it created in COMSOL is shown in figs. 2b and 2d (necessary assumptions were made for dimensions not mentioned in the paper).

3 Linear analysis

Linear analysis was performed based on which the intended axis stiffness and full stiffness matrix were computed. Material properties of PLA were employed.

3.1 Intended-axis stiffness

A moment about Z axis was applied to the mobile end and the rotational displacement was computed based on which the compliance relevant about this dof for a load applied at this dof is computed to be:

$$C_{\theta_z\theta_z} = 0.521 \text{ (Nm)}^{-1},$$
$$k^*_{\theta_z\theta_z} = 1.92 \text{ Nm},$$

where $k^*_{\theta_z\theta_z}$ is the intended axis stiffness (close to the value of 2.03 Nm obtained in [2]).

3.2 Full stiffness matrix

The full compliance matrix (only for the single dof in the node of interest-center of mobile plate in fig. 2) is calculated by assigning a load and then measuring the displacement. The full compliance matrix for the node is then calculated.

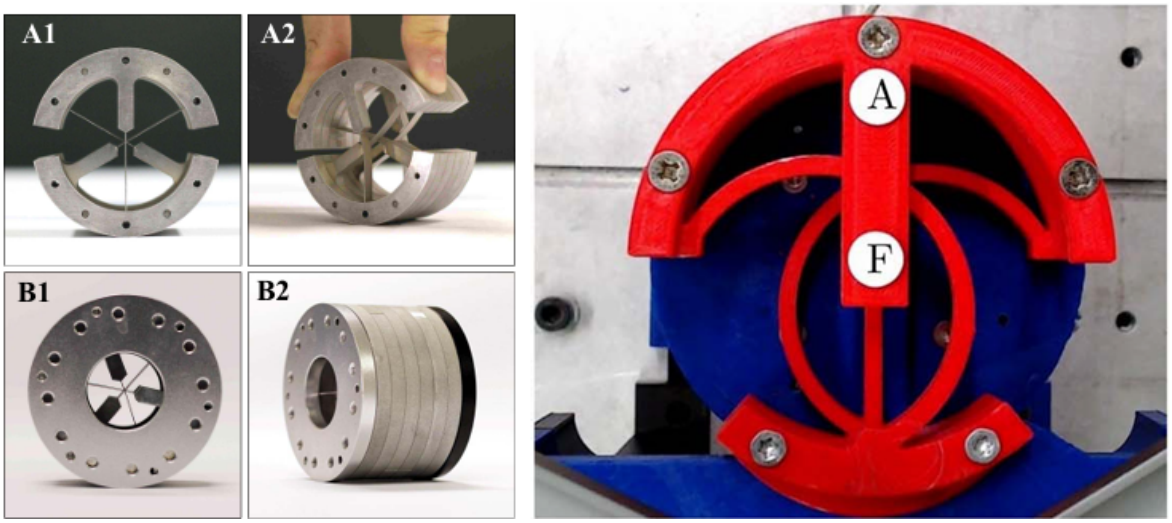

(a) TaCP with straight elements, Image taken from Ref.[1]

(b) TaCP with curved elements, Image taken from Ref.[2]

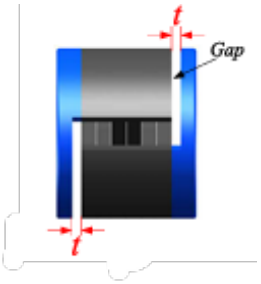

(c) Side view of a general TaCP, Image taken from Ref.[1]

Figure 1: Triple-axis cross pivot

$$\bar{\mathbf{C}} = \begin{bmatrix} c_{\theta_x\theta_x} & c_{\theta_x\theta_y} & c_{\theta_x\theta_z} & c_{\theta_x x} & c_{\theta_x y} & c_{\theta_x z} \\ c_{\theta_y\theta_x} & c_{\theta_y\theta_y} & c_{\theta_y\theta_z} & c_{\theta_y x} & c_{\theta_y y} & c_{\theta_y z} \\ c_{\theta_z\theta_x} & c_{\theta_z\theta_y} & c_{\theta_z\theta_z} & c_{\theta_z x} & c_{\theta_z y} & c_{\theta_z z} \\ c_{x\theta_x} & c_{x\theta_y} & c_{x\theta_z} & c_{xx} & c_{xy} & c_{xz} \\ c_{y\theta_x} & c_{y\theta_y} & c_{y\theta_z} & c_{yx} & c_{yy} & c_{yz} \\ c_{z\theta_x} & c_{z\theta_y} & c_{z\theta_z} & c_{zx} & c_{zy} & c_{zz} \end{bmatrix} =$$

$$\begin{bmatrix} 1.61E-01 & 3.45E-04 & -2.81E-02 & -6.50E-04 & -3.32E-03 & -1.15E-04 \\ 7.25E-05 & 2.13E-01 & 9.70E-04 & 4.46E-03 & 2.79E-05 & 1.56E-05 \\ -2.81E-02 & 9.73E-04 & 5.21E-01 & -4.53E-03 & 6.04E-04 & -1.61E-05 \\ -6.50E-04 & 4.46E-03 & -4.53E-03 & 2.01E-04 & 1.46E-05 & 5.03E-07 \\ -3.33E-03 & 2.70E-05 & 6.04E-04 & 1.46E-05 & 7.25E-05 & 3.88E-07 \\ -1.70E-04 & 1.65E-05 & -1.64E-05 & 5.01E-07 & 5.12E-07 & 6.30E-05 \end{bmatrix},$$

,

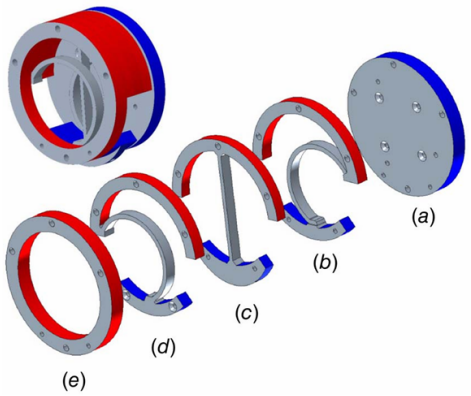

(a) Geometry of TaCP (Δ configuration) modeled in Serafino et al. [2], red faces are held fixed and blue faces are connected to the mobile part.

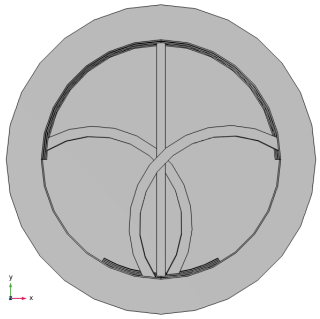

(b) Geometry modeled in COMSOL (top view)

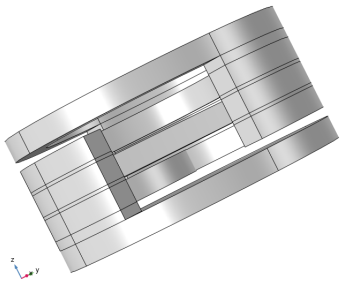

(c) Geometry modeled in COMSOL (side view)

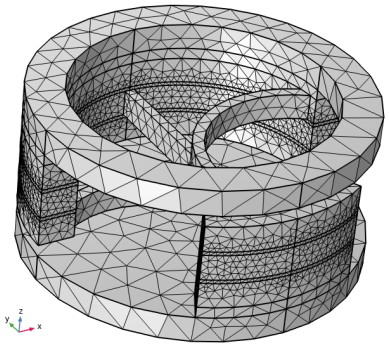

(d) Mesh employed in study (Verification of independence of result on mesh size is performed for linear study)

Figure 2: Geometry of triple-axis cross pivot

$$\bar{\mathbf{K}} = \bar{\mathbf{C}}^{-1} = \begin{bmatrix} k_{\theta_x\theta_x} & k_{\theta_x\theta_y} & k_{\theta_x\theta_z} & k_{\theta_x x} & k_{\theta_x y} & k_{\theta_x z} \\ k_{\theta_y\theta_x} & k_{\theta_y\theta_y} & k_{\theta_y\theta_z} & k_{\theta_y x} & k_{\theta_y y} & k_{\theta_y z} \\ k_{\theta_z\theta_x} & k_{\theta_z\theta_y} & k_{\theta_z\theta_z} & k_{\theta_z x} & k_{\theta_z y} & k_{\theta_z z} \\ k_{x\theta_x} & k_{x\theta_y} & k_{x\theta_z} & k_{xx} & k_{xy} & k_{xz} \\ k_{y\theta_x} & k_{y\theta_y} & k_{y\theta_z} & k_{yx} & k_{yy} & k_{yz} \\ k_{z\theta_x} & k_{z\theta_y} & k_{z\theta_z} & k_{zx} & k_{zy} & k_{zz} \end{bmatrix} =$$

$$\begin{bmatrix} 125.58 & -1.66 & 0.41 & 34.17 & 5746.88 & 193.87 \\ -1.29 & 11.66 & -3.01 & -332.38 & 28.66 & -3.53 \\ 0.30 & -3.01 & 3.24 & 143.54 & -40.93 & 1.23 \\ 22.37 & -332.37 & 143.54 & 15869.30 & -3241.41 & 53.09 \\ 5757.52 & 11.51 & -36.05 & -2702.74 & 278557.73 & 8793.69 \\ 291.69 & -5.76 & 1.88 & 112.02 & 13222.53 & 16334.40 \end{bmatrix}$$

where $\mathbf{C}_{ij} = \frac{\Delta_i}{F_j}$, $k_{u_i u_i}$ is in units of N/m, $k_{u_i\theta_i}$ is in units of N and $k_{\theta_i\theta_i}$ is in units of Nm (for elements in compliance matrix units are in inverse of unit of respective element in stiffness matrix).

Noticing the 3$^{\text{rd}}$ column in the compliance matrix we notice for moment along z axis, the unintended rotational displacements are much smaller (more than an order of magnitude) than the rotational displacement along intended axis, also we notice that x displacement is around 4.53 mm for a rotational displacement of 0.521 rad (around 30°) which is significant drift and might restrict use of this device in applications where drift is critical (arguments made based on extrapolation from linear analysis, which is verified thorugh nonlinear analysis in the next section).

4 Nonlinear analysis

Nonlinear analysis is performed for same geometry. Images of solution at different loads is shown in appendix.

4.1 Extent of linearity

The variation of rotational displacement of the mobile plate w.r.t. fixed plate for different applied moment is shown in fig. 3.
Based on the figure we can see that the response is almost linear till 30° (similar to what was observed in [2]).

4.2 Axis-drift

The variation of axis drift (z-axis passing through center of mobile disk) for different applied moment (in terms of rotational displacement) is shown in fig. 4a.
There is a significant axis drift which is worsened at higher loads (the pattern matches what is reported in [2] but the values are higher than what is observed, possibly due to a difference in dimension of certain elements).

4.3 Range of rotation

The variation of maximum von-Mises stress observed in the domain at different rotational displacements are shown in fig. 4b.
Assuming an yield strength of 60MPa for PLA, the material fails roughly at 24° rotational displacement. No buckling of elements was observed (which is also evidenced in the smooth nature of load-displacement plot in fig. 3).

5 Conclusions

The performance of triple-axis cross pivot as an elastic pair is studied and relevant parameter of interest were calculated.

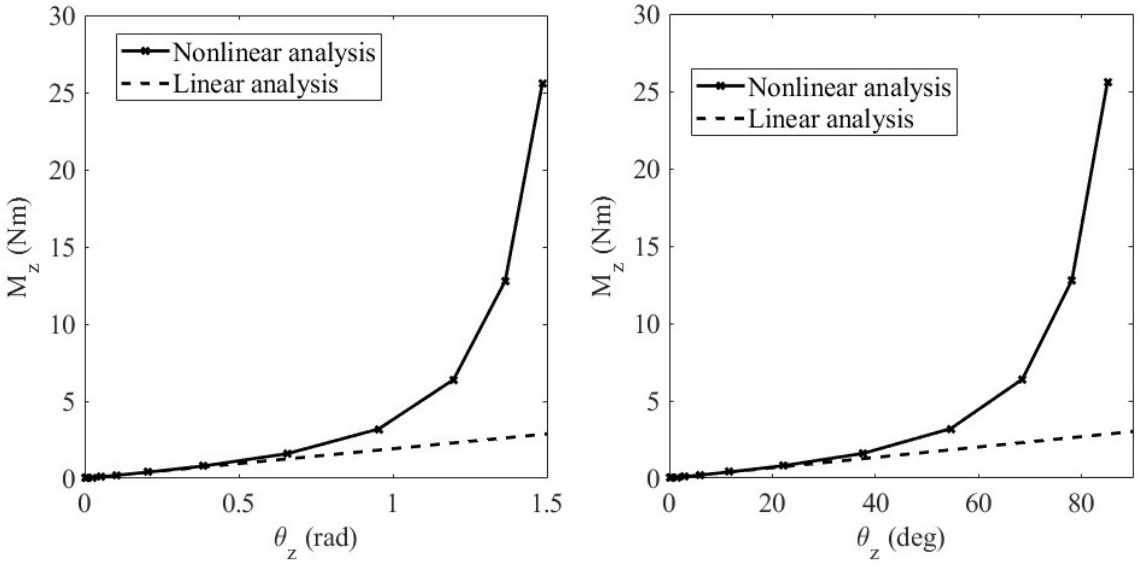

Figure 3: Variation of rotational displacement with torsional moment

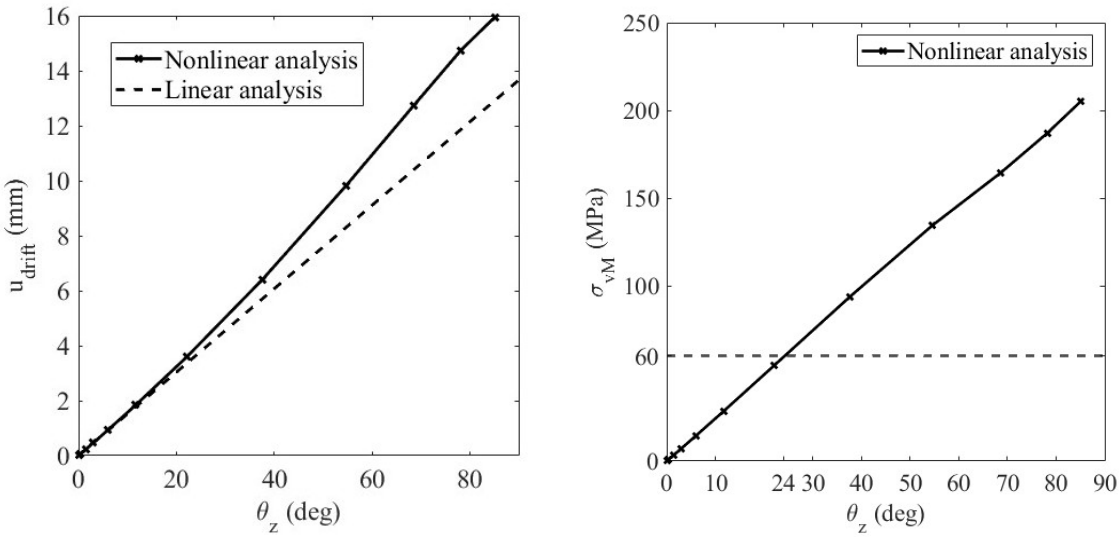

(a) Axis drift

(b) Maximum von-Mises stress

Figure 4: Variation of parameters with rotational displacement

6 Appendix

The response of elastic pair to forces/moments along intended and unintended directions studied through linear analysis is shown in fig. 5.
The response of elastic pair to different magnitudes of torsional moment studied through nonlinear analysis is shown in fig. 6.

References

[1] L. Liu, S. Bi, Q. Yang, and Y. Wang. Design and experiment of generalized triple-cross-spring flexure pivots applied to the ultra-precision instruments. *Review of Scientific Instruments*, 2014. doi: 10.1063/1.4897271.

[2] S. Serafino, L. Bruzzone, P. Fanghella, and M. Verotti. Design of high-performance triple-axis cross pivots. *Journal of Mechanisms and Robotics*, 2024. doi: 10.1115/1.4065749.

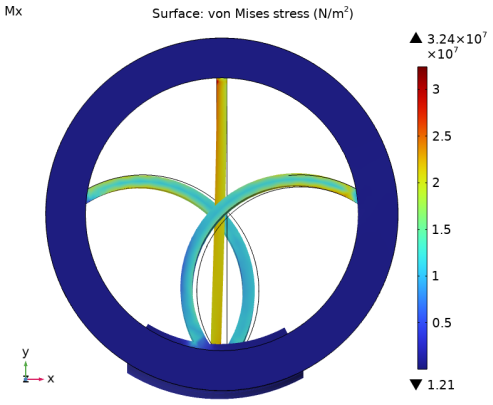

(a) M_x-Top view

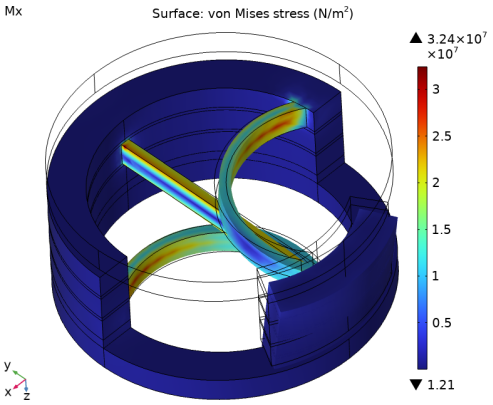

(b) M_x-Side view

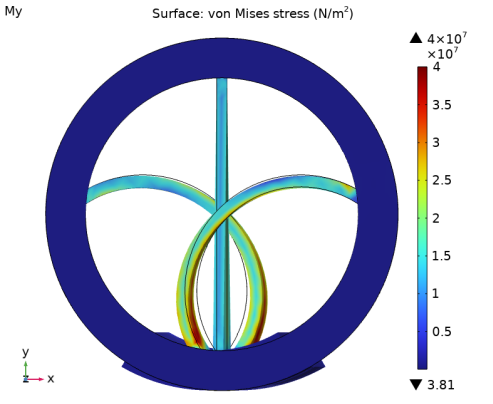

(c) M_y-Top view

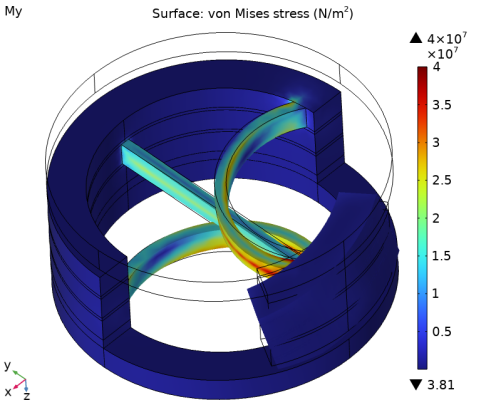

(d) M_y-Side view

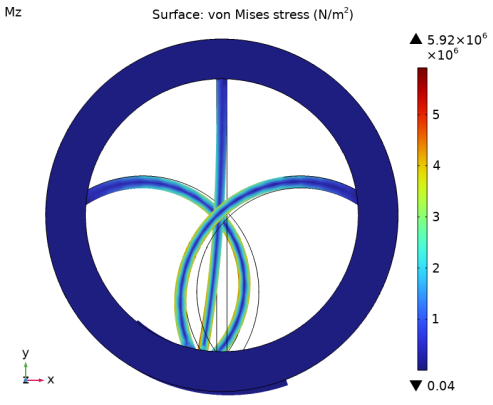

(e) M_z-Top view

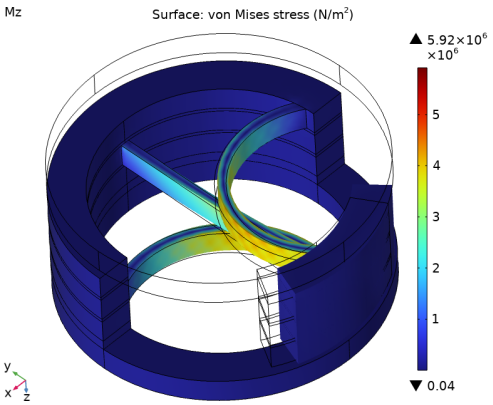

(f) M_z-Side view

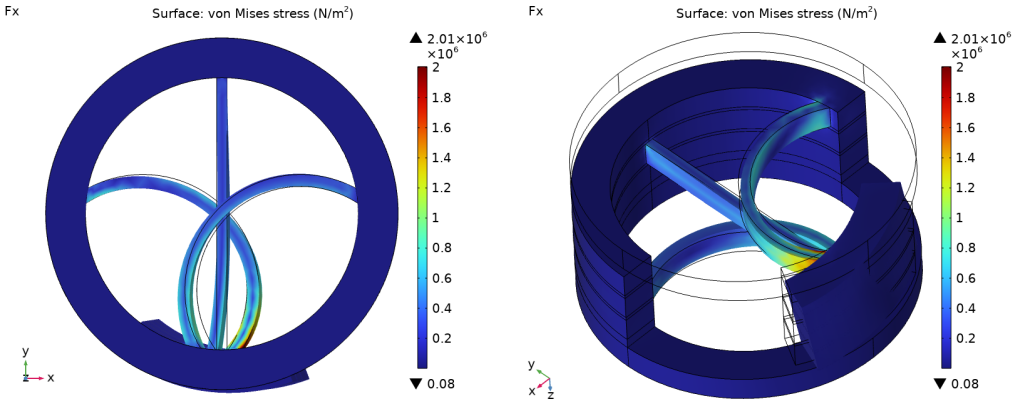

(g) F_x-Top view

(h) F_x-Side view

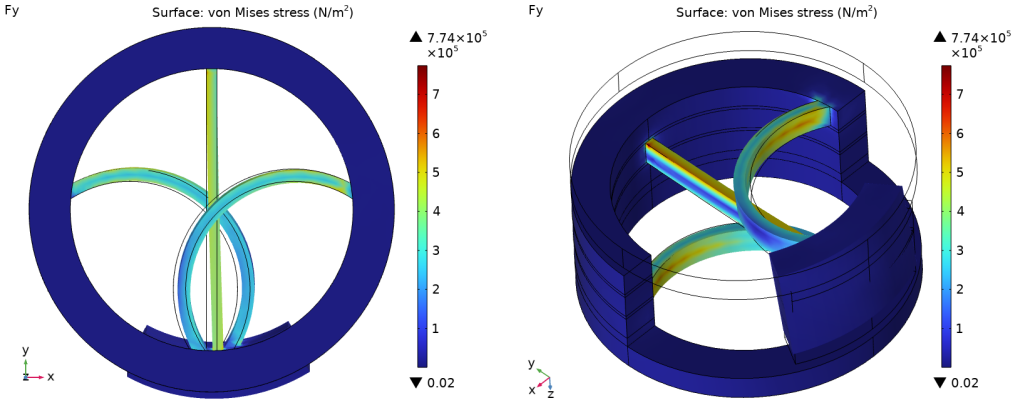

(i) F_y-Top view

(j) F_y-Side view

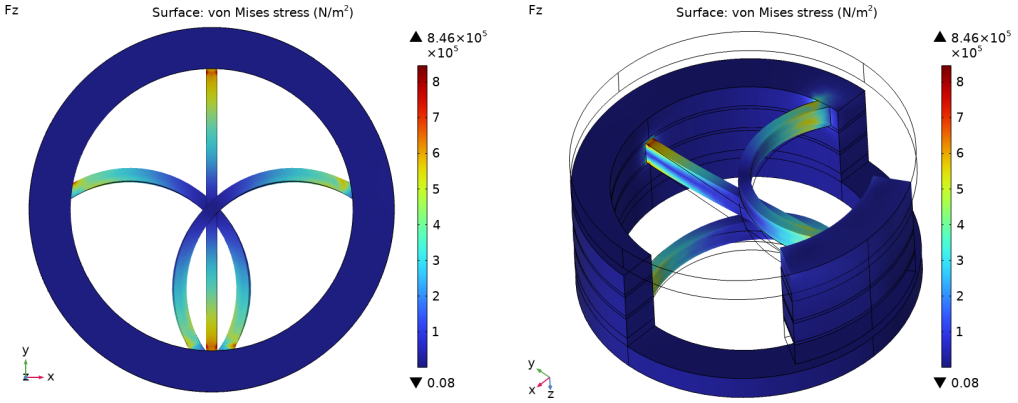

(k) F_z-Top view

(l) F_z-Side view

Figure 5: Response of elastic pair to forces/moments along specified directions (scaled appropriately)

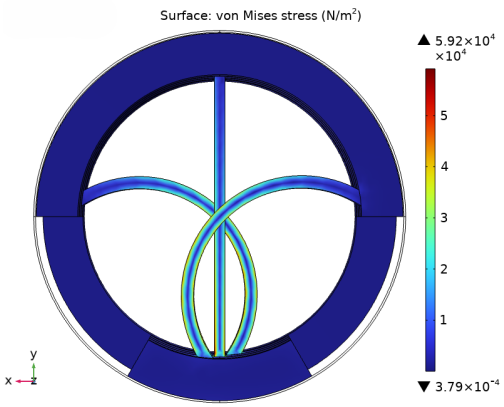

(a) M_z=0.001 Nm, θ_z=0.03°

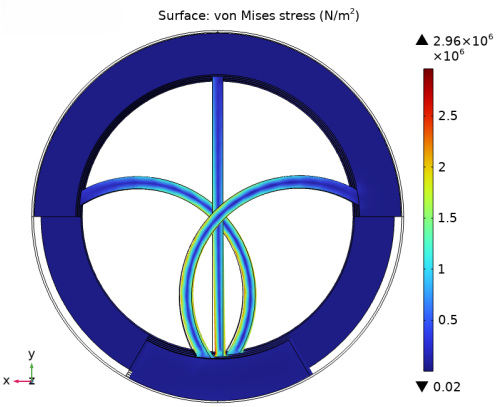

(b) M_z=0.01 Nm, θ_z=0.30°

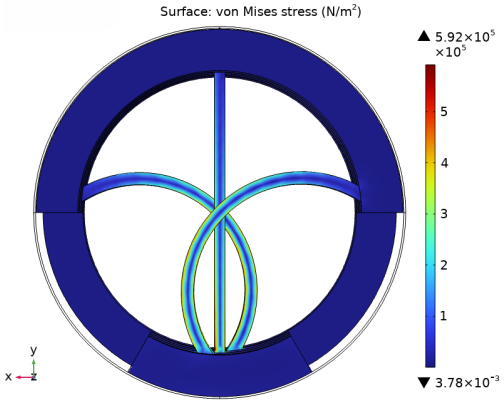

(c) M_z=0.05 Nm, θ_z=1.49°

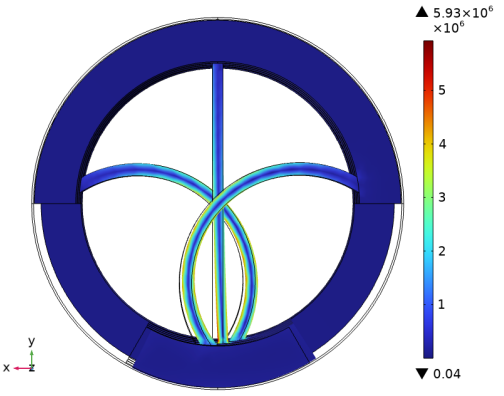

(d) M_z=0.1 Nm, θ_z=2.98°

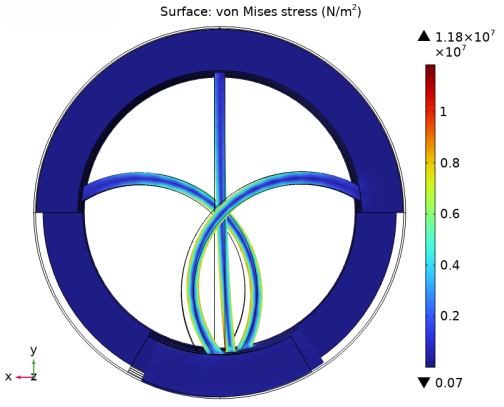

(e) M_z=0.2 Nm, θ_z=5.94°

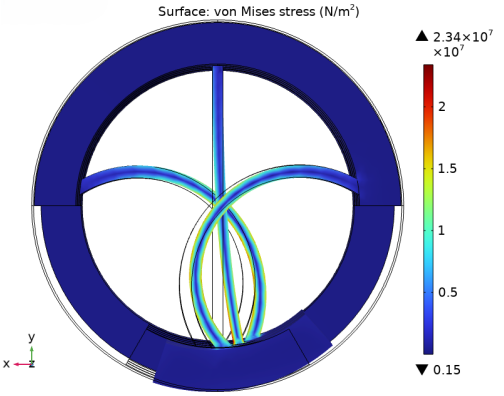

(f) M_z=0.4 Nm, θ_z=11.69°

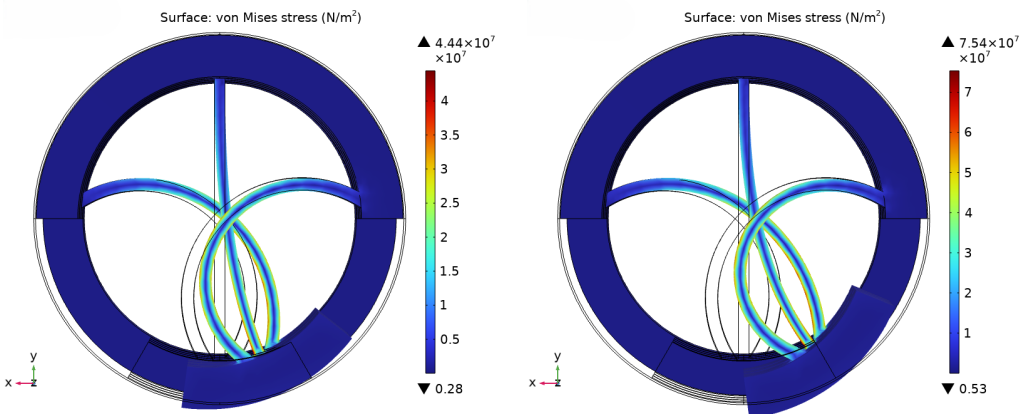

(g) M_z=0.8 Nm, θ_z=22.10°

(h) M_z=1.6 Nm, θ_z=37.65°

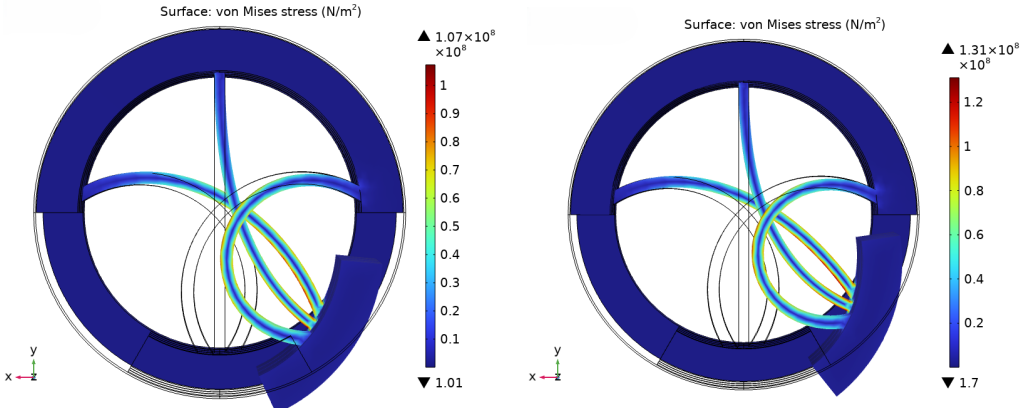

(i) M_z=3.2 Nm, θ_z=54.66°

(j) M_z=6.4 Nm, θ_z=68.59°

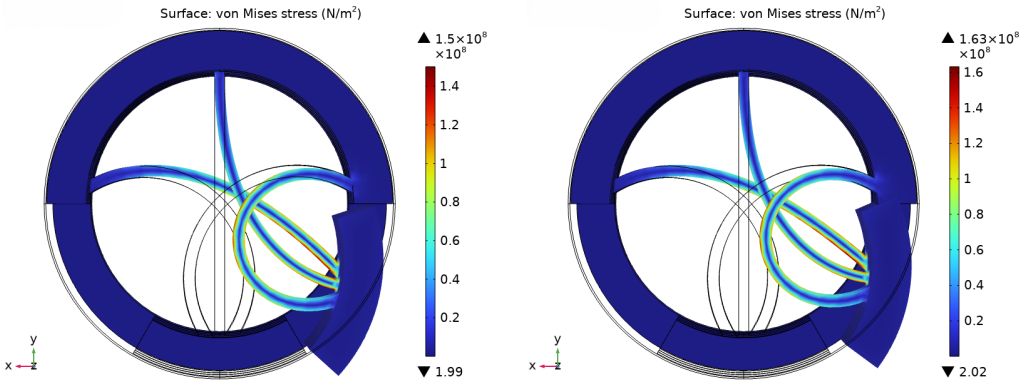

(k) M_z=12.8 Nm, θ_z=78.20°

(l) M_z=25.6 Nm, θ_z=85.10°

Figure 6: Response of elastic pair to different magnitudes of torsional moment (unscaled)